Swimming efficiency of bacterium *Escherichia coli*

Suddhashil Chattopadhyay*, Radu Moldovan*, Chuck Yeung†, and X. L. Wu*‡

*Department of Physics and Astronomy, University of Pittsburgh, Pittsburgh, PA 15260; and †School of Science, Behrend College, Pennsylvania State University, Erie, PA 16563

Edited by Howard C. Berg, Harvard University, Cambridge, MA, and approved July 26, 2006 (received for review March 13, 2006)

We use measurements of swimming bacteria in an optical trap to determine fundamental properties of bacterial propulsion. In particular, we directly measure the force required to hold the bacterium in the optical trap and determine the propulsion matrix, which relates the translational and angular velocity of the flagellum to the torques and forces propelling the bacterium. From the propulsion matrix, dynamical properties such as torques, swimming speed, and power can be obtained by measuring the angular velocity of the motor. We find significant heterogeneities among different individuals even though all bacteria started from a single colony. The propulsive efficiency, defined as the ratio of the propulsive power output to the rotary power input provided by the motors, is found to be ≈2%, which is consistent with the efficiency predicted theoretically for a rigid helical coil.

bacterial flagellum | bacterial propulsion | propulsion matrix

Bacteria swim by rotating helical propellers called flagellar filaments. For *Escherichia coli* (*E. coli*), these filaments are several micrometers in length and 20 nm in diameter, organized in a bundle of four or five. Each flagellar filament is driven at its base by a reversible rotary engine, which turns at a frequency of ≈100 Hz (1). Many important properties of the swimming bacteria, such as their average swimming speed, the rotation rate of the flagellar bundle, and the torque generated by the molecular motor, have been determined (1–5, 23). Other properties such as the translational and rotational drag coefficients of flagellar bundles, however, are difficult to measure, especially for intact cells. These parameters are significant for quantitative understanding of bacterial propulsion and are the subject of extensive mathematical analysis and computer simulations (6–10). In this work, we investigate the fundamental swimming properties of intact *E. coli* by using optical tweezers and an imposed external flow. We directly measure the force required to hold the bacterium and the angular velocities of the flagellar bundle and the cell body as a function of the flow velocity. The propulsion matrix, which relates the translational and angular velocity of the flagella to the forces and torques propelling the bacterium, can thus be determined one bacterium at a time. We find that the population-averaged matrix elements are in reasonable agreement with the resistive force theory for helical propellers (7), but there is a large variability even among bacteria of similar length grown from a single colony.

The propulsion matrix also allows us to determine the propulsive efficiency ε, which is defined as the ratio of the propulsive power output (the part of the power used to push the cell body forward) to the rotary power input (the power used to rotate the flagellar bundle). We find the propulsive efficiency is strongly dependent on growth conditions but is not very sensitive to cell-body size. Despite the flexibility and internal friction between the filaments in the flagellar bundle, the measured efficiency of ≈2% is close to the maximum efficiency for the given cell body and shape of the flagella filament and is consistent with the 1–3% efficiency predicted theoretically for a rigid helical coil (9). Our experimental technique is versatile and can be used to make comparative studies of bacteria under different growth conditions, mutant strains of the same species, or different microorganisms. Such measurements can shed light on how this remarkable ability to swim evolves among different microorganisms.

Propulsion Matrix

Bacterial swimming occurs at very low Reynolds numbers ($Re \simeq 10^{-4}$) such that the fluid motion is governed by Stokes flow, and nonlinearities in the full hydrodynamic equation are irrelevant. For peritrichously flagellated bacteria such as *E. coli*, the flagellar bundle may be approximated as a single effective propeller. Despite these simplifying features, the problem remains theoretically difficult because of complicated time-dependent boundary conditions. Theoretical studies, therefore, usually assume that the flagellar filaments have very simple geometries such as an infinite sheet (6) or a helical coil (7, 9). For more realistic modeling, one must rely on numerical methods (11). A second approach is not to take into account specific geometries but to consider general relations appropriate in the low Reynolds-number limit for a rigid object (10). In this regime, the torque $N_{\rm fl}$ acting on the propeller and the thrust force $F_{\rm thrust}$ generated by it are linearly related to the propeller's angular velocity ω and the translational velocity v (relative to the background fluid) as follows:

$$-F_{\rm thrust} = Av - B\omega, \qquad \textbf{[1a]}$$

$$N_{\rm fl} = -Bv + D\omega. \qquad \textbf{[1b]}$$

The above equations can be expressed in terms of the symmetric propulsion matrix,

$$P = \begin{bmatrix} A & -B \\ -B & D \end{bmatrix},$$

also known as the resistance matrix (12). By using the coordinate system in Fig. 1, $F_{\rm thrust}$ and v are positive if directed toward the head of the cell, while the sign of ω and $N_{\rm fl}$ obeys the right-hand rule; i.e., the flagellar filament is a left-handed helix. The coefficients A, B, and D are positive, proportional to fluid viscosity η, and depend on the shape and size of the propeller. The basic physics is that in the absence of an applied torque, a translating propeller under the influence of an external force must rotate, and in the absence of an applied force, a rotating propeller under the influence of an external torque must translate (10).

The propulsive matrix description is applicable to propellers of any shape and size. However, for a rigid helical coil, the matrix elements can be derived from resistive force theory (7) with the result:

$$A = K_n \ell \frac{1-\beta}{\beta^{1/2}} \left(1 + \gamma_k \frac{\beta}{1-\beta}\right), \qquad \textbf{[2a]}$$

Conflict of interest statement: No conflicts declared.

This paper was submitted directly (Track II) to the PNAS office.

‡To whom correspondence should be addressed at: Department of Physics and Astronomy, University of Pittsburgh, 100 Allen Hall, 3941 O'Hara Street, Pittsburgh, PA 15232. E-mail: xlwu@pitt.edu.

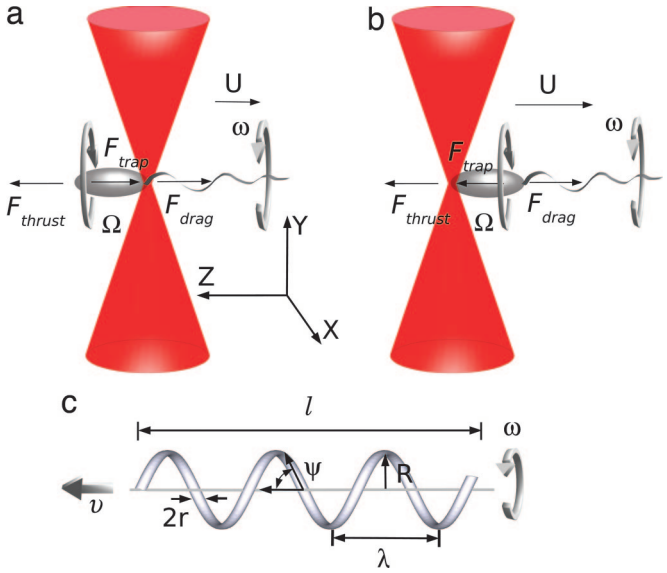

Fig. 1. Two different trapping configurations are possible. (*a*) The bacterium can be trapped horizontally at the tail of the cell body in the absence of a flow, $U = 0$, and for a small negative U; i.e., $|U| < V_{swim}$, where V_{swim} is the free-swimming speed of the bacterium. (*b*) The bacterium can also be stably trapped at the head of the cell body in the presence of a larger negative U, i.e., $|U| > V_{swim}$. The forces and velocities are positive if they are along $+Z$. The rotations are defined by the right-hand rule such that $\omega < 0$ and $\Omega > 0$ as depicted. (*c*) A schematic of an effective helical propeller: ℓ is the length, $2r$ is the diameter of the filament, R is the radius, Ψ is the pitch angle of the helix relative to the swimming axis, and λ is the pitch.

$$B = K_n \ell \left(\frac{\lambda}{2\pi}\right) \frac{1-\beta}{\beta^{1/2}} (1-\gamma_k), \qquad [2b]$$

$$D = K_n \ell \left(\frac{\lambda}{2\pi}\right)^2 \frac{1-\beta}{\beta^{1/2}} \left(1+\gamma_k \frac{1-\beta}{\beta}\right), \qquad [2c]$$

where ℓ is the length of the coil, λ is the pitch, and $\beta = \cos^2\Psi$ with Ψ being the pitch angle relative to the swimming axis (see Fig. 1*c*). By using λ and Ψ, the radius of the helical coil is given by $R = (\lambda/2\pi)\tan\Psi$. The quantity γ_k is the ratio of the tangential viscous coefficient $K_t = 4\pi\eta/(2\ln(c\lambda/r) - 1)$ to the perpendicular viscous coefficient $K_n = 8\pi\eta/(2\ln(c\lambda/r) + 1)$, where r is the radius of the coil filament and c is a constant. For a smooth filament, Lighthill (7) showed using a mean-field approximation, $c \simeq 0.18$ and $\gamma_k = K_t/K_n \approx 0.7$, where the experimental data ($\lambda/r \simeq 100$) from sea-urchin spermatozoa was used (8). The helix loses its ability to propel if $\gamma_k \to 1$, $\Psi \to 0$ ($\beta \to 1$), or $\Psi \to \pi/2$ ($\lambda \to 0$) as expected.

To complete the description of the swimming bacterium, we need the propulsion matrix P_0 for the cell body. Unlike P for the flagellum, P_0 is diagonal ($B_0 = 0$) because the cell body cannot propel itself. The nonviscous force on the cell body consists of two parts, the trapping force F_{trap} due to the optical tweezers holding the bacteria and the thrust F_{thrust} generated by the flagella. The sum of these forces must balance the viscous force $A_o v$ acting on the cell body. Likewise, the nonviscous torque acting on the cell body $-N_{fl}$ must balance the viscous rotational drag. The above consideration gives the following:

$$F_{trap} + F_{thrust} = A_0 v, \qquad [3a]$$

$$D_0\Omega = -N_{fl}, \qquad [3b]$$

where Ω is the angular velocity of the cell body. We treat the cell body as a prolate spheroid with minor semiaxis a and major semiaxis b. If the cell body is in the bulk of the fluid, the linear and rotational drag coefficients are then $A_0 = 4\pi\eta b/(\ln(2b/a) - (1/2))$ and $D_0 = 16\pi\eta a^2 b/3$ (13). The optical trapping force is harmonic $F_{trap}(z) = -k(z - z_0)$, where k is the spring constant and $z - z_0$ is the displacement from the center of the trap (14, 15). Because the bacteria is held by the optical tweezers, its net velocity in the lab frame is 0 ($v' = v + U \simeq 0$), and the relative velocity v to the fluid is opposite to the external flow U. Substituting $v = -U$ into Eqs. **1** and **3** gives the following:

$$k(z - z_0) = (A + A_0)U + B\omega, \qquad [4a]$$

$$D_0\Omega = -BU - D\omega. \qquad [4b]$$

This set of equations will be used below to analyze our data.

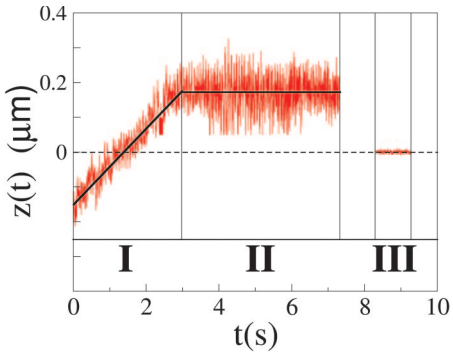

Fig. 2. A typical experimental run for a swimming bacterium held in the optical trap. In regime I, an uniform flow $U = -40$ μm/s is decreased to zero linearly with time. The flow U remains zero in regime II. The laser is blocked momentarily to let the bacterium escape, and the undeflected laser beam position is recorded in regime III. The solid lines depict linear fits to each regime.

Results

We used a nontumbling strain of *E. coli* bacteria HCB30 in our measurements. We found that a swimming bacterium near a glass surface could be stably trapped by the optical tweezers along its swimming direction. The bacterium is then manipulated by an imposed uniform external flow U. Fig. 1 illustrates our experimental setup along with the flow configurations. A bacterium swimming to the left (along the $+Z$ direction) is held by a strongly focused IR laser (λ = 1,064 nm). In the absence of flow, the bacterium is invariably held at the tail of the cell body as shown in Fig. 1*a*. The thrust and trapping forces are balanced, and the bacterium is stationary with respect to the trap. The bacterium remains trapped at the tail for small negative U ($-U < V_{swim}$). For larger flow speeds, the bacterium becomes trapped at the head of the cell body as shown in Fig. 1*b*.

To measure the trapping force and the position of the trapped cell tip, the transmitted IR beam was refocused and projected onto a two-dimensional position-sensitive detector. This technique allowed us to measure the position of the trapped cell tip with respect to the center of the trap. A nonflagellated bacterium (YK4516) was used to calibrate the spring constant k of the optical trap. A description of the calibration and measurement procedure is presented in *Materials and Methods*.

Fig. 2 displays an example of the time trace $z(t)$ of the longitudinal displacement of the trapped cell tip along the swimming direction of the bacterium. We observed large oscillations overlying a systematic variation of $z(t)$ as the external flow is changed. These oscillations result from wobbling of the cell body in response to the rotation of the flagellar bundle (4, 16). The trapped bacterium was perturbed by the following sequence of events. In regime I, U is linearly reduced from -40 μm/s to

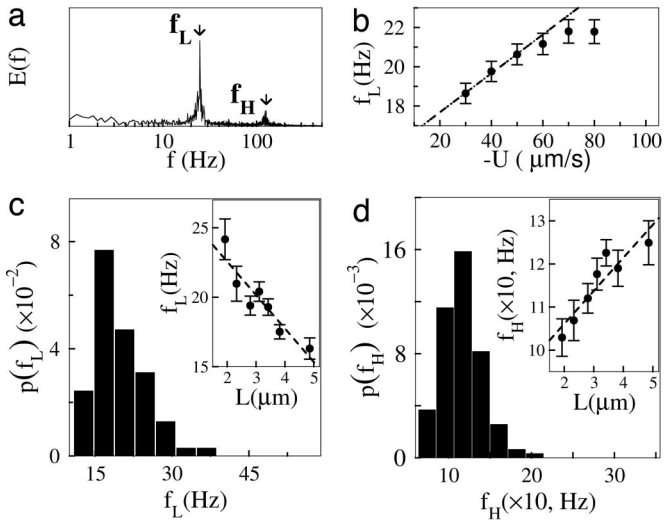

Fig. 3. Rotational motion of the cell body and the flagellar bundle. (*a*) Power spectrum of $E(f)$ of $x(t)$ shows peaks corresponding to f_L and f_H. (*b*) The variation of the rotation frequency of the cell body f_L as a function of flow speed $-U$. The linear dependence is consistent with the propulsion matrix formulation. Error bars are SEM unless otherwise noted. (*c* and *d*) The PDFs of f_L (*c*) and f_H (*d*) are delineated. (*Insets*) The average f_L and f_H as a function of cell-body length L.

0 in 3 s. If the flow speed $|U|$ is larger than the free swimming speed $V_{\rm swim}$, the bacterium is trapped at the head (Fig. 1*b*), and $z(t) < 0$. When $|U| \leq V_{\rm swim}$, the bacterium swims forward, becomes trapped at the tail of the body (Fig. 1*a*), and $z(t) > 0$. The zero crossing point ($z(t) = 0$) occurs precisely when $|U| = V_{\rm swim}$. In regime II, U is maintained at 0 for 4 s, and the average position of the bacterium relative to the trap is constant. Finally, in regime III, the bacterium is released by temporarily blocking the laser beam. The position of the undeflected beam in regime III is taken to be z_o, the center of the optical trap. From regime I we obtain the net translational drag coefficient $A + A_0 = k\Delta z/\Delta U$, and in regime II we obtain $F_{\rm thrust}$, because $F_{\rm trap} = -F_{\rm thrust}$ when $U = 0$. We checked that the measurement was reproducible by returning the flow to $U = -40$ μm/s rather than releasing the bacterium after regime II. The bacterium returned to within a few percent of its initial average position.

We used transverse oscillations $x(t)$, which were more pronounced than $z(t)$, to obtain the angular velocity of the cell body and the flagellar bundle. Fig. 3*a* displays a sample power spectrum $E(f)$ of $x(t)$ for a short time interval of 4 s when $U = 0$. The power spectrum has two strong peaks at $f_L \simeq 25$ Hz and $f_H \simeq 124$ Hz, respectively. These two frequencies can be associated with the angular velocities of the cell body $\Omega = 2\pi f_L$ and of the flagellar bundle $\omega = -2\pi f_H$ (16). Averaging over 200 bacteria, we found $\bar{f}_{\rm L} = 19.6 \pm 0.3$ Hz and $\bar{f}_{\rm H} = 115 \pm 2$ Hz, where the standard errors of the mean (SEM) are quoted. As shown in Fig. 3 *c* and *d*, there is considerable variation of f_L and f_H between individual bacteria; the standard deviations (SD) $\sigma_{f_L} = 5.4$ Hz and $\sigma_{f_H} = 25$ Hz are, respectively, 28% and 22% of the mean values. As suggested by Fig. 3 *c Inset* and *d Inset*, some of the variation is due to dependence of f_L and f_H on the cell-body length $L \equiv 2b$; namely, the cell-body rotation frequency f_L decreases whereas the flagellar rotation frequency f_H increases as L is increased. Because the motor angular velocity is defined as $\Omega_m \equiv \Omega - \omega = 2\pi(f_L + f_H)$, we found that Ω_m increases slightly with L.

To test the basic physics implied by the propulsion matrix, we measured the dependence of f_L and f_H on U for an additional 150 bacteria, which were subjected to flow speeds of $-U = 30$, 40, 50, 60, 70, and 80 μm/s. Fig. 3*b* shows that the average frequency $\bar{f}_{\rm L}$ increases linearly with small $|U|$, but the rate of increase decreases considerably for $|U| > 60$ μm/s. The linear dependence for small $|U|$ is in good agreement with Eq. **4**, which is an essential property of the propulsion-matrix formulation. The deviation for large $|U|$ represents a nonlinear response of the cell to the flow and is likely due to deformations of flagellar bundles at a high speed.[§] Within the noise of the measurement, no systematic change in $\bar{f}_{\rm H}$ was detected.

To complete our determination of the propulsion matrix, the semiminor axis a and the length L of the bacterial cell body were measured directly by video microscopy while the bacterium was held in the trap. The procedure allows us to calculate the drag coefficients A_0 and D_0 for the cell body. However, because the bacteria were trapped approximately $d \simeq 5$ μm above a solid surface, wall effects must be taken into account. By using the analysis of Happel and Brenner (12), the wall corrections to the drag coefficients are given by an expansion in terms of the ratio of the characteristic body size L to the distance d from the wall with the result $A_0 \simeq A_0(\infty)[1 - \kappa_1 A_0(\infty)/(6\pi\eta d) + O(L/d)^3]^{-1}$ and $D_0 \simeq D_0(\infty)[1 - \kappa_2 D_0(\infty)/(8\pi\eta d^3) + O(L/d)^5]^{-1}$. Here, $A_0(\infty) = 2\pi\eta L/(\ln(L/a) - (1/2))$ and $D_0(\infty) = 8\pi\eta a^2 L/3$ are the bulk values when $L/d \to 0$, and $\kappa_1 = 9/16$ and $\kappa_2 = 1/8$ are constants. A straightforward calculation based on the mean bacterial size and our experimental geometry shows that A_0 and D_0 are increased by 13% and 4% from their bulk values, respectively. However, the approximation is marginal for the largest-size bacteria studied. The above conclusion indicates that the surface effect, although not negligible, is not significant enough to qualitatively alter the propulsion-matrix representation. In other words, we expect that the linear relation in Eq. **4** still holds approximately and the values of A, B, and D are moderately different from their bulk values. From the time trace $z(t)$, A and B are calculated by $A = k\Delta z/\Delta U - A_0$ (regime I) and $B = F_{\rm thrust}/\omega$ (regime II). Finally, the measurements of the angular velocities give $D = -(\Omega/\omega)D_0$.

The calculations were repeated for the 200 bacteria. The average values of the matrix elements were $\bar{A} = (1.48 \pm 0.04) \times 10^{-8}$ N·s/m, $\bar{B} = (7.9 \pm 0.2) \times 10^{-16}$ N·s, and $\bar{D} = (7.0 \pm 0.1) \times 10^{-22}$ N·s·m. The translational drag coefficient of the flagellar bundle is approximately equal to that of the cell body ($\bar{A}_0 = 1.4 \times 10^{-8}$ N·s/m). Therefore, approximately half of the drag on the bacteria is due to the flagella. On the other hand, the rotational drag of the flagella $\bar{D}$ is much smaller than that of the cell body ($\bar{D}_0 = 4.2 \times 10^{-21}$ N·s·m).

The theoretical expressions for A, B, and D given in Eq. **2** can then be used to extract physical parameters of the flagellar bundle if we treat the bundle as a single effective flagella. This abstraction is consistent with the observation that the flow field induced by a model rotating bundle is very close to that induced by a rotating rigid helix of appropriate thickness (18). In principle, the expressions in Eq. **2** should also be corrected for surface effects. However, such corrections will be complex and are beyond the scope of this work. Therefore, in the following analysis, it is assumed that the measured A, B, and D are unaffected by the surface. As we will show, important physical parameters that are extracted from our measurements, such as the pitch and helix length, are in reasonably good agreement with existing measurements (19), indicating that surface corrections to A, B, and D are moderate.

[§]By using simple dimensional analysis, we expect that deformation takes place when $\Pi \simeq K_n \ell^3 U$, where $\Pi \simeq 10^{-23}$ J·m is the bending elastic modulus (17). By using $\ell \simeq 7$ μm for the length of the flagellum and $K_n \simeq 10^{-3}$ kg·s^{-1}·m^{-1}, we estimate that bending is significant when $U \simeq 30$ μm/s. This estimate is not too far from our measured value of 60 μm/s. However, this estimate is very rough because Π is only known to an order of magnitude, and the nonlinearity could also be due to other effects such as improper bundle formation at high flow speeds.

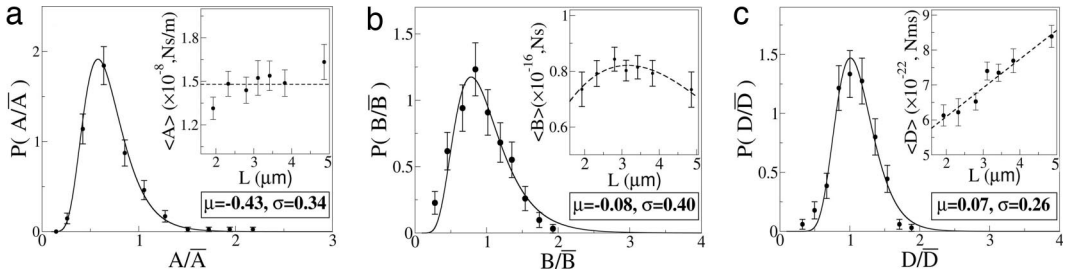

Fig. 4. The PDFs of $A/\bar{A}$ (*a*), $B/\bar{B}$ (*b*), and $D/\bar{D}$ (*c*). The solid lines are fits to the log-normal distribution $P(x) = \exp[-(\ln x - \mu)^2/2\sigma^2]/(x\sigma\sqrt{2\pi})$. The fitting parameters μ and σ are given in the plots. (*Insets*) The bacterial length L dependence of $\langle A\rangle$ (*a*), $\langle B\rangle$ (*b*), and $\langle D\rangle$ (*c*).

The resistive force theory for the helix coil contains four independent parameters: the pitch λ, the pitch angle Ψ, the length of the helix ℓ, and the radius r of the filament, assuming that the viscosity of the fluid ($\eta = 10^{-3}$ Pa·s) is known. The three matrix elements A, B, and D in Eq. **2** are not sufficient to predict all four parameters (λ, Ψ, ℓ, and r). To make progress, we assumed that the pitch angle Ψ is 41°, as determined by Turner *et al.* (19) using fluorescently labeled *E. coli* cells. This angle is very close to the angle (42°) that maximizes the propulsion efficiency of an ideal helix (7). By using our measured $\bar{A}$, $\bar{B}$, $\bar{D}$, and $\beta = \cos^2(41°) = 0.57$, Eq. **2** predicts $\gamma_k = 0.61$, $\ell = 6.5$ μm, and $\lambda = 1.5$ μm. The two geometrical parameters ℓ and λ are in reasonable agreement with the fluorescent measurements of Turner *et al.* (19), who found $\bar{\ell} = 7$ μm and $\bar{\lambda} \simeq 2$ μm for the normal form of flagella. The value of γ_k we obtained is ≈13% smaller than estimated by Lighthill (7). By using our measured γ_k and assuming $r \simeq 20$ nm for a flagellar bundle consisting of three or four flagella, we found $c \simeq 2.4$, which is nearly a factor of 10 greater than that calculated by Lighthill (7) using a self-consistent argument. Surprisingly, c estimated from this experiment is closer to the original value, $c = 2$, suggested by Gray and Hancock (8).

All important dynamical quantities can be obtained from our measurements. For example, the average thrust for $U = 0$ is $\bar{F}_{\rm thrust} = \bar{B}\bar{\omega} = 0.57$ pN, whereas the average torque is $\bar{N}_{\rm fl} = \bar{D}\bar{\omega} = 5 \times 10^{-19}$ N·m, which is close to that found for bacteria *Streptococcus* (4). The calculated mean swimming speed $\bar{V}_{\rm swim} = \bar{B}\bar{\omega}/(\bar{A}_0 + \bar{A}) = 20.4$ μm/s agrees well with direct measurements of the average swimming speed using video microscopy, $\bar{V}_{\rm swim} \approx 22$ μm/s. Additional measurements further showed that $\bar{V}_{\rm swim}$ was the same before and after trapping, indicating minimal photo effects in this horizontal trapping configuration.

The propulsion matrix elements vary greatly among individual bacteria, even though they were grown from a single colony. Fig. 4 displays the probability distribution functions (PDFs) of the scaled quantities $A/\bar{A}$, $B/\bar{B}$, and $D/\bar{D}$. The SD σ are significant fractions of the means with $\sigma_A/\bar{A} \simeq 40\%$, $\sigma_B/\bar{B} \simeq 37\%$, and $\sigma_D/\bar{D} \simeq 27\%$. A conspicuous feature of the PDFs is their broad tails, particularly for A and B. Such a feature might be an indication of structural heterogeneities in the flagellar bundles of individual cells or that the conformation of the bundles changes with time. As is often the case in biological systems, the PDFs with broad tails can be roughly fitted to log-normal distributions that are plotted as solid lines in Fig. 4.

Part of the variations in A, B, and D must arise because the bacteria are in different stages of their growth cycle during the measurements. This is especially the case for the early log phase of a growing culture, where the bacterial size is large and highly varied. In the present experiment, the bacteria were grown to the midlog phase (≈4.5 h growth time), where bacteria are smaller and their size distribution is narrower. However, even at this stage, the cells are far from homogeneous. Fig. 5*a* shows the cell-length distribution of the group of 200 randomly selected bacteria. The fitted PDF (solid line) is peaked at ≈3 μm with an SD of 0.8 μm. The figure also shows the smallest cell length L_0 at which a septal ring becomes discernible. We used the bacterial length L as a measure of its physiological state and determined the propulsive matrix elements as a function of L. To improve the statistics for large L, a centrifugation technique was used to select long bacteria ($4 < L < 6$ μm; $n = 50$). We determine the length dependence of the coefficients A, B, and D by calculating the averaged values $\langle A\rangle$, $\langle B\rangle$, and $\langle D\rangle$ for bacteria of similar length L. The results are presented in Fig. 4 *Insets*. The linear drag coefficient $\langle A\rangle$ has no clear size dependence, but $\langle B\rangle$ has a small peak at $L \approx 3.3$ μm, which coincides with the peak of the bacterial size L distribution. On the other hand, Fig. 4*c* shows that the rotational drag coefficient $\langle D\rangle$ of the propeller increases linearly with L.

These size dependencies allow us to draw certain conclusions about the structure of flagellar bundles at different stages of cell growth. Inspection of Eq. **2** shows that the three matrix elements are similar in their dependence on parameters such as the pitch angle Ψ (or β) and γ_k. Such similarity precludes the possibility that β and γ_k are controlling the different L dependencies seen

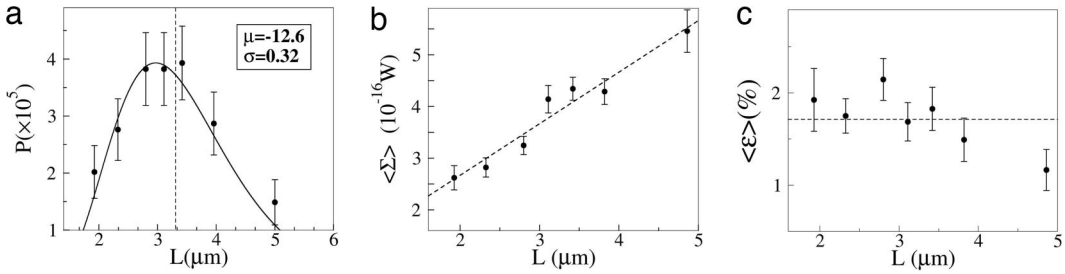

Fig. 5. Bacterial size dependence. (*a*) The PDF of the bacterial cell length L. The solid line is a fit to the log-normal distribution with the parameters σ and μ defined in Fig. 4. The vertical line marks the smallest cell length L_0 at which we observed a septal ring. (*b*) The flagellar power output $\langle\Sigma\rangle$ as a function of L. The dashed line is a linear fit. (*c*) The propulsion efficiency $\langle\varepsilon\rangle$ as a function of L. The dotted horizontal line marks the mean efficiency 1.7% of the entire population of 250 bacteria.

in the measurements. On the other hand, the matrix elements depend strongly on the pitch λ with $A \propto \lambda^0$, $B \propto \lambda^1$, and $D \propto \lambda^2$. These relationships correlate with the observation that A has the least and D has the most L dependence. The observation therefore implies that the primary L dependence is through the pitch λ. One may thus conclude that both β and γ_k are approximately constant for different sized bacteria, which is physically and biologically reasonable. Because our measurements show a linear relation between D and L, one can also conclude that λ^2 grows linearly with L. A possible scenario is that as the cell body elongates, more flagella are incorporated into the bundle, and consequently its stiffness and λ increase. From the shortest to the longest bacterial body length (2–5 μm), we found that the fractional change $\delta\lambda/\lambda$ should be ≈18%, which may be discernible in carefully conducted observations using fluorescently labeled bacteria.

We next turned our attention to the power and propulsive efficiency of the swimming bacteria. The average power output of the flagellar motors is $\bar{\Sigma} = \bar{D}_0\bar{\Omega}|\bar{\omega} - \bar{\Omega}| = 4.3 \times 10^{-16}$ W. The power used to turn the cell body is $\bar{D}_0\bar{\Omega}^2 \approx 6.3 \times 10^{-17}$ W, whereas the actual propulsive power is another factor of 10 smaller with $\bar{A}_0\bar{V}_{\rm swim}^2 \approx 5.8 \times 10^{-18}$ W. Therefore, ≈15% of the rotary power is used to rotate the cell body; only ≈1.3% is used to push the bacteria forward; and the rest is dissipated as heat. Fig. 5*b* shows the average motor power as a function of bacterial length L. The power increases gradually with L, which is consistent with the above discussion that the number of flagella and the associated motors increase with L. The propulsion efficiency ε, defined as the ratio of the propulsive output power to the rotary input power, can be related to the propulsion matrix elements (10) as follows:

$$\varepsilon \equiv \frac{A_0 v^2}{N_{\rm fl}(\omega - \Omega)} = \frac{A_0 D_0 B^2}{[(A_0 + A)D - B^2][(A_0 + A)(D_0 + D) - B^2]}. \quad [5]$$

Fig. 5*c* shows that the efficiency as a function of bacterial size is nearly constant up to $L \simeq 4$ μm. The average efficiency is $\bar{\varepsilon} \approx 1.7\%$, which is slightly larger than the 1.3% estimated above. The discrepancy is due to correlations between A, B, and D of individual cells, i.e., $\varepsilon(\bar{A}, \bar{B}, \bar{D})$ is not the same as $\bar{\varepsilon}(A, B, D)$ when evaluated using Eq. **5**. Our measured efficiencies are surprisingly close to the 1–3% predicted theoretically for a rigid helical propeller (7, 9). Similar measurements were also carried out for bacteria grown to an early log phase. In this case, although the average swimming speed is approximately a factor of 3 lower ($\bar{V}_{\rm swim} \simeq 6$ μm/s), the swimming efficiency reduces by almost a factor of 10 with $\bar{\varepsilon} \simeq 0.2\%$. This efficiency is comparable with the $\bar{\varepsilon} \simeq 0.35$–$0.7\%$ found by Purcell (10) using helical coils made of metal wires. The lower efficiency observed by Purcell is likely due to the suboptimal pitch angle of the coils used.

We can also ask the following for a given A_0: What is the maximum efficiency attainable by the bacterium as a function of the length of the flagellum ℓ? Assume that at some characteristic length ℓ_p, the propulsive coefficients of the flagellar bundle are A_p, B_p, and D_p. Assuming that the width of the bundle is constant, these coefficients should grow linearly with the flagellar length ℓ so that $A \approx \kappa A_p$, $B \approx \kappa B_p$, and $D \approx \kappa D_p$, where $\kappa = \ell/\ell_p$. This assumption is consistent with Eq. **2**. Substituting for A, B, and D into our expression for ε (in Eq. **5**) and assuming $B^2 \ll (A_0 + A)D$ and $D_0 \gg D$, we find that the maximum efficiency occurs when $A = A_0$ and $\varepsilon_{\rm max} \approx B_p^2/(4A_pD_p)$, which depends only on the shape of the propeller. The same result was obtained by Purcell (10) when he maximized ε by assuming that all propeller dimensions (not just the length) scaled with κ. In our experiment, we found that $\bar{A}$ is approximately equal to $\bar{A}_0$ so that flagella are as long as required to maximize its propulsive efficiency.

Summary

In summary, bacterial propulsion is investigated by using optical tweezers, which allow us to directly measure the thrust force $F_{\rm thrust}$ as a function of the imposed flow. For a free swimming bacterium, $F_{\rm thrust}$ precisely balances the viscous drag of the cell body $A_0 v$ and of the flagellar bundle Av. Unlike the viscous drag of the cell body, the contribution of the flagellar bundle to the total drag is difficult to determine without direct force measurements such as the one presented here. We showed that the propulsion matrix proposed by Purcell (10) gives an adequate description of bacterial swimming over a physiological range of velocities. In retrospect, this finding is not obvious considering that flagellar filaments are tenuous and are deformable because of hydrodynamic stress induced by swimming or by flows (20, 21). Indeed, our measurements do show nonlinear response to changes in U when a strong flow ($|U| > 3V_{\rm swim}$) is imposed.

We have determined all elements of the propulsion matrix and used the resistive force calculations for a helical coil to estimate microscopic properties of the flagellar bundle (7). The measured geometric parameters such as ℓ and λ are consistent with earlier measurements using fluorescently labeled bacteria (19). The parameter $c \simeq 2.4$ is significantly greater than Lighthill's (7) self-consistent calculation ($c = 0.18$) but comes closer to the original estimate ($c = 2$) of Gray and Hancock (8). By using the propulsion matrix, we also determined dynamic quantities related to bacterial swimming and their dependence on the size of the cell body. In particular, we found that the propulsive efficiency ε, defined as the ratio of the propulsive power output to the rotary power input, is ≈1.7%. This efficiency depends weakly on the bacterial size but strongly on the growth condition. The measured ε is close to the maximum efficiency for the given size of the cell body and the shape of the flagellar bundle. Our results suggest that resistive force theory has captured essential physics of bacterial swimming, and complications such as long-range hydrodynamic interactions between different flagellar filaments and of the filaments with the cell body are too subtle to be discernible in the present investigation.

Materials and Methods

Sample Preparation. We followed standard growth conditions for culturing bacteria *E. coli* strains, HCB30 and YK4516. A single colony was picked from a fresh agar plate and grown to saturation overnight in tryptone broth (4 g of peptone/1 g of NaCl/0.4 ml of 1 M NaOH in 400 ml of water). The culture was maintained at 33°C and was shaken continuously at 200 rpm. The overnight sample was diluted to 1:100 in fresh tryptone broth and grown to the midlog phase for 4.5 h. The sample was next washed by centrifugation at room temperature (Model 5415D, Eppendorf, Westbury, NY; 1,400 rpm, 5 min) and resuspended gently in a motility medium [10 mM KPO_4/0.1 mM EDTA/0.1 mM glucose/0.0002% (wt/vol) Tween 20]. Experiments were carried out after a dilution of 1:300 in the same motility medium.

Measurements. The swimming bacterium was held by a strongly focused IR laser (λ = 1,064 nm) a few micrometers above the glass surface. We found that in the interior of the fluid, without flow, the bacterium could only be stably trapped in the vertical direction, along the trapping axis. In this configuration, it was feasible to determine the threshold of the trapping force and relate it to the maximum of the thrust (22). However, the method is not suitable for measuring instantaneous thrust force acting on the cell body. The presence of a surface is necessary to hold the bacterium in the horizontal position, and the thrust is monitored continuously as a function of time. Although the physics of such a stable trap is not understood at present, we believe that both

steric and hydrodynamic interactions between the cell and the wall play a role. To measure the trapping force and the position of the trapped cell tip, the transmitted IR beam was refocused by a high numerical aperture condenser (N.A. 1.5) and projected onto a two-dimensional position sensitive detector (Model DL100-7PCBA; Pacific Silicon Sensor, Inc., Westlake Village, CA). The position of the trapped cell tip with respect to the center of the trap was monitored by a PC equipped with an analog–digital converter card (Model AT-MIO-16E-2; National Instruments, Austin, TX). The conversion rate was 5 kHz at 12-bit resolution.

A nonflagellated bacterium (YK4516) was used to calibrate the spring constant k of the optical trap by measuring the position of the trapped tip as a function of the flow speed U. For the nonflagellated bacteria, a uniform flow was necessary to hold the bacteria in the horizontal position. The uniform flow U was set up by translating the sample chamber, using a DC motor controller (Model 855; Newport, Irvine, CA) and a motorized translation stage. For an ellipsoid body, the translational drag coefficient A_o is known, and the spring constant can be obtained by using $k = A_o \Delta U/\Delta z$. For the laser intensity (20 mW) used in this experiment, $k = 5.7 \times 10^{-6}$ N/m. This calculation gives a roll-off frequency $f_C (\equiv k/2\pi A_0) \simeq 63$ Hz, which was indeed seen in the experiment. The noise in the output of the optical trap was 0.1 nm/$\sqrt{\text{Hz}}$, for $z_{\text{rms}} = 5.2$ nm and a sampling rate of 5 kHz.

We thank Howard Berg and Linda Turner (both of Harvard University, Cambridge, MA) for thoughtful comments and suggestions and for the gift of the bacterial strain HCB30 used in this experiment and Emily Chapman, Bob Duda, and Roger Hendrix for helpful discussions and technical assistance. This work was supported by National Science Foundation Grant DMR-0242284.

1. Samuel ADT, Berg HC (1996) *Biophys J* 71:918–923.
2. Macnab RM (1992) *Annu Rev Genet* 26:131–158.
3. Meister M, Lowe G, Berg HC (1987) *Cell* 49:643–650.
4. Lowe G, Meister M, Berg HC (1987) *Nature* 325:637–640.
5. Chen X, Berg HC (2000) *Biophys J* 78:1036–1041.
6. Taylor GI (1952) *Proc R Soc London Ser A* 211:225–239.
7. Lighthill J (1989) *Mathematical Biofluiddynamics* (SIAM, Philadelphia), 3rd Ed.
8. Gray J, Hancock GJ (1955) *J Exp Biol* 32:802–814.
9. Childress S (1981) *Mechanics of Swimming and Flying*, Cambridge Studies in Mathematical Biology (Cambridge Univ Press, New York), 1st Ed.
10. Purcell EM (1997) *Proc Natl Acad Sci USA* 9:11307–11311.
11. Ramia M, Tullock DL, Phan Thien N (1993) *Biophys J* 65:755–778.
12. Happel J, Brenner H (1981) *Low Reynolds Number Hydrodynamics* (Springer, New York), 1st Ed.
13. Berg HC (1993) *Random Walks in Biology* (Princeton Univ Press, Princeton), 1st Ed.
14. Wuite GJ, Davenport RJ, Rappaport A, Bustamante C (2000) *Biophys J* 79:1155–1167.
15. Neuman KC, Block SM (2004) *Rev Sci Instrum* 75:2787–2809.
16. Rowe AD, Leake MC, Morgan H, Berry RM (2003) *J Mod Opt* 50:1539–1554.
17. Fujime S, Maruyama M, Asakura S (1972) *J Mol Biol* 68:347–354.
18. Kim MJ, Bird JC, Park J, Powers TR, Breuer KS (2004) *Exp Fluids* 37:782–788.
19. Turner L, Ryu WM, Berg HC (2000) *J Bacteriol* 182:2793–2801.
20. Macnab RM, Ornston MK (1977) *J Mol Biol* 112:1–30.
21. Hotani H (1982) *J Mol Biol* 156:791–806.
22. McCord RP, Yukich JN, Bernd KK (2005) *Cell Motil Cytoskeleton* 61:137–142.
23. Magariyama Y, Sugiyama S, Kazumasa M, Kawagishi I, Imae Y, Kudo S (1995) *Biophys J* 69:2154–2162.